ACS OMEGA

http://pubs.acs.org/journal/acsodf

Article

Evaluation of ^{89}Zr-Labeled Anti-PD-L1 Monoclonal Antibodies Using DFO and Novel HOPO Analogues as Chelating Agents for Immuno-PET

Bhasker Radaram,[○] Sarah E. Glazer,[○] Ping Yang, Chia-Wei Li, Mien-Chie Hung, Seth T. Gammon, Mian Alauddin, and David Piwnica-Worms*

Cite This: *ACS Omega* 2023, 8, 17181−17194

Read Online

ACCESS | Metrics & More | Article Recommendations | Supporting Information

ABSTRACT: Programmed death ligand 1 (PD-L1) is a type 1 transmembrane immunosuppressive protein that is expressed on a wide range of cell types, including cancer cells. Anti-PD-L1 antibodies have revolutionized cancer therapy and have led to improved outcomes for subsets of cancer patients, including triple-negative breast cancer (TNBC) patients. As a result, PET imaging of PD-L1 protein expression in cancer patients has been explored for noninvasive detection of PD-L1 expressing tumors as well as monitoring response to anti-PD-L1 immune checkpoint therapy. Previous studies have indicated that the *in vivo* stability and *in vivo* target detection of antibody-based radio-conjugates can be dramatically affected by the chelator used. These reports demonstrated that the chelator HOPO diminishes ^{89}Zr de-chelation compared to DFO. Herein, we report an improved HOPO synthesis and evaluated a series of novel analogues for thermal stability, serum stability, PD-L1-specific binding using the BT-549 TNBC cell line, PET imaging *in vivo*, as well as biodistribution of ^{89}Zr-labeled anti-PD-L1 antibodies in BT-549 xenograft murine models. A new chelator, C5HOPO, demonstrated high stability *in vitro* and afforded effective PD-L1 targeting *in vivo via* immuno-PET. These results demonstrated that an improved HOPO chelator is an effective chelating agent that can be utilized to image therapeutically relevant targets *in vivo*.

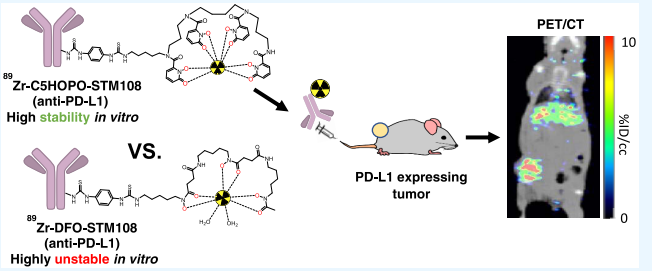

INTRODUCTION

Immunoglobulin-like immunosuppressive proteins, such as programmed death ligand 1 (PD-L1; also known as B7 homologue 1), are expressed on a wide range of cell types, including cancer cells.[1] PD-L1 binds the receptor programmed cell death protein 1 (PD-1), leading to the inhibition of T-cell proliferation, cytolytic activity, and overall immune response. Complexation of PD-L1 with PD-1 hinders the activation state of CD28/major histocompatibility complex (MHC) and results in inhibition of T-cell proliferation.[2,3] Clinical trials have demonstrated that targeting the PD-L1/PD-1 axis with monoclonal antibodies rejuvenates tumor-infiltrating lymphocytes.[4−7] Several monoclonal antibodies that target either PD-1 or PD-L1 have been developed and used for cancer immunotherapy,[8−10] including nivolumab and pembrolizumab, which target PD-1 and atezolizumab, durvalumab, and avelumab, which target PD-L1.[11−13] Advanced combination therapies are underway, for example, a phase III clinical trial study from IMpassion130 demonstrated efficacy and safety when using atezolizumab plus nab-paclitaxel (immunotherapy in combination with chemotherapy) to treat patients with PD-L1 immune cell-positive unresectable, locally advanced or metastatic triple-negative breast cancer (TNBC).[14] This is particularly encouraging as TNBC, defined based on the lack of expression of estrogen (ER), progesterone (PR), or HER2 receptors, is the most aggressive breast cancer phenotype with the poorest outcome. Many combination studies are ongoing.[15−18]

These results point to opportunities to develop new immuno-PET imaging agents for both PD-L1 assessments in TNBC patients and for use in monitoring response to immunotherapy. Previous work has demonstrated that PET imaging of radiolabeled anti-PD-L1 antibodies may offer significant advantages in analyzing PD-L1 protein expression *in vivo* compared to conventional immunohistochemistry, which has many limitations, including the need for an invasive biopsy, often provides inaccurate quantification of PD-L1 expression in metastatic and damaged tissues, and is unable to detect changes in PD-L1 expression due to dynamic changes in the tumor microenvironment.[19−21] In addition, anti-PD-L1 antibody PET

Received: March 7, 2023
Accepted: March 24, 2023
Published: May 4, 2023

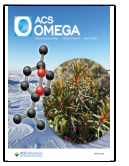

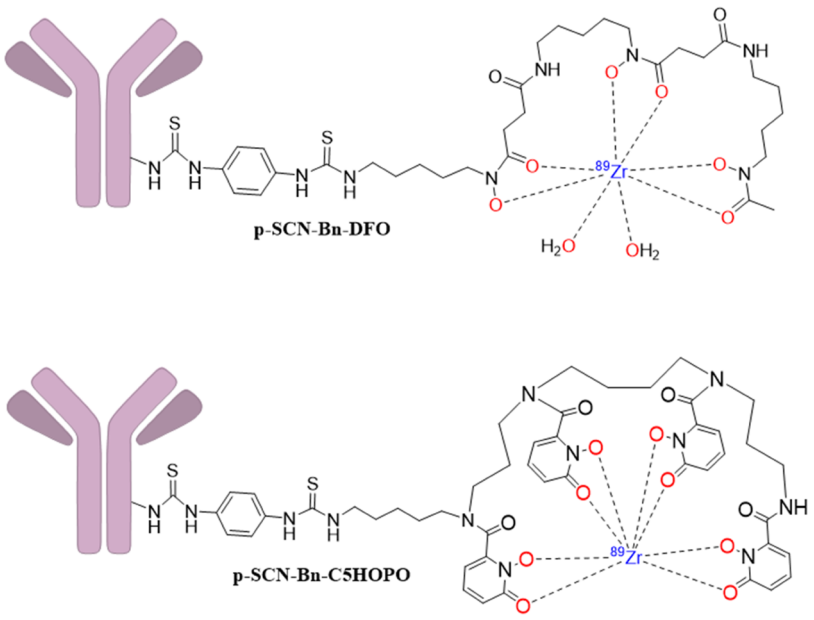

Figure 1. Chemical structures of ^{89}Zr-*p*-SCN-Bn-DFO and the novel ^{89}Zr-*p*-SCN-Bn-C5HOPO conjugated with a representative monoclonal antibody.

imaging can evaluate both primary tumors and metastasis, potentially alleviating the false negative rate in mulitfocal disease and identifying toxicities due to bone marrow or spleen binding *via* a noninvasive imaging procedure.[22−31]

Several immuno-PET agents, *i.e.*, positron-emitting radionuclides linked by a bifunctional chelator that has been conjugated to a monoclonal antibody, have been developed over the past several years.[32] Zirconium-89 (^{89}Zr), a positron-emitting radionuclide, has received much attention for use in antibody-based PET imaging[33,34] because of its relatively long half-life (78.4 h), which is compatible with the biological half-life of antibodies, and its relatively low-energy positron (β_{avg} = 395.5 keV), which affords high-resolution images and allows collection of a large number of images. Several ^{89}Zr-based antibody imaging agents have been translated into clinical trials.[34−40] Thus, further advancement of anti-PD-L1 antibodies radiolabeled with positron-emitting isotopes may be useful for PET imaging in order to monitor treatment response to immunotherapy in PD-L1 immune-positive patients.

Several chelators have gained attention in recent years capable of sequestering longer-lived radiometals relevant to immuno-PET.[41] A well-known standard bifunctional chelator for ^{89}Zr is desferrioxamine B (DFO), a bacterial siderophore and hexadentate ligand consisting of three hydroxamates that provide six oxygen donors (3 anionic and 3 neutral) for radiometal binding. DFO has a hexadentate capacity to form a complex with ^{89}Zr.[42−44] Raavé et al.[45] recently reported the modification of DFO for the complexation of ^{89}Zr. Still, Deri et al.[46] reported that DFO may not be an ideal ligand for ^{89}Zr because the uptake of radioactivity in the bone is high owing to the accumulation of $^{89}Zr^{4+}$ in the skeleton due to possible de-chelation, as demonstrated when ^{89}Zr was conjugated specifically to trastuzumab, an anti-HER2 receptor antibody.[47,48] De-chelation of radioactivity and deposition into the bone cortex and marrow is especially problematic as the bone marrow is a radiosensitive tissue. This observed de-chelation *in vivo* may limit the use of DFO as a chelator for ^{89}Zr. Deri and colleagues also reported synthesizing a new bifunctional chelator for ^{89}Zr, 3,4,3-(LI-1,2-HydrOxyPyridinOne) (HOPO).[46] A non-hydroxamate-based ligand, HOPO consists of four 1,2-hydroxypyridinones for metal binding (*i.e.*, Zr^{4+}) as an octadentate chelator (*i.e.*, 8 oxygen donors, 4 anionic and 4 neutral) with spermine as a backbone (Figure 1). ^{89}Zr-HOPO-trastuzumab was found to be a stable complex with lower bone activity than the DFO conjugate. Tinianow et al.[49] also reported that the ^{89}Zr-HOPO complex showed less bone retention than did ^{89}Zr-DFO.

Herein, we report an improved alternative synthesis of three novel HOPO ligands with various carbon-chain lengths to link the backbone of HOPO to a para isothiocyanate phenylthiourea moiety used for the conjugation to proteins and monoclonal antibodies. The *in vitro* thermal and serum stabilities of the novel HOPO ligands chelated to zirconium-89 were evaluated. Finally, the most stable and easy-to-use ligand, C5HOPO, was conjugated to two anti-PD-L1 antibodies, STM004 and STM108,[50] and we evaluated these new anti-PD-L1 radioconjugates *in vitro*, and *in vivo* in a murine xenograft model of TNBC.

RESULTS AND DISCUSSION

Synthesis and Characterization of Novel HOPO Analogues. First, we described an improved synthetic strategy leading to three novel HOPO analogues with three different carbon chain lengths, hereafter known as C3HOPO, C4HOPO, and C5HOPO. *N*-Protected amino-alkyl iodides **5a-c** (Scheme S3) of three different carbon chain lengths (n = 1, 2, and 3) were prepared in three steps, with an overall yield of 70%. The reaction of spermine with *N*-protected amino-alkyl iodides **5a-c** yielded mono-substituted spermine **6a-c** with up to 81% yield (Scheme S4). The reaction between the mono-substituted spermine derivatives **6a-c** and HOPO acid chloride **9a** (1-(benzyloxy)-6-oxo-1,6-dihydropyridine-2-carbonyl chloride) was carried out *in situ* by treating compound **9** (Scheme S5) with oxalyl chloride and yielded *N*-protected amino-alkyl spermine-HOPO derivatives **10a-c** with a 23% yield in 5 h, relatively faster compared to the literature methods.[46,51] The

https://doi.org/10.1021/acsomega.3c01547
ACS Omega 2023, 8, 17181−17194

Scheme 1. Synthetic Scheme for the Preparation of *p*-NCS-Bn-HOPO (12a-c)

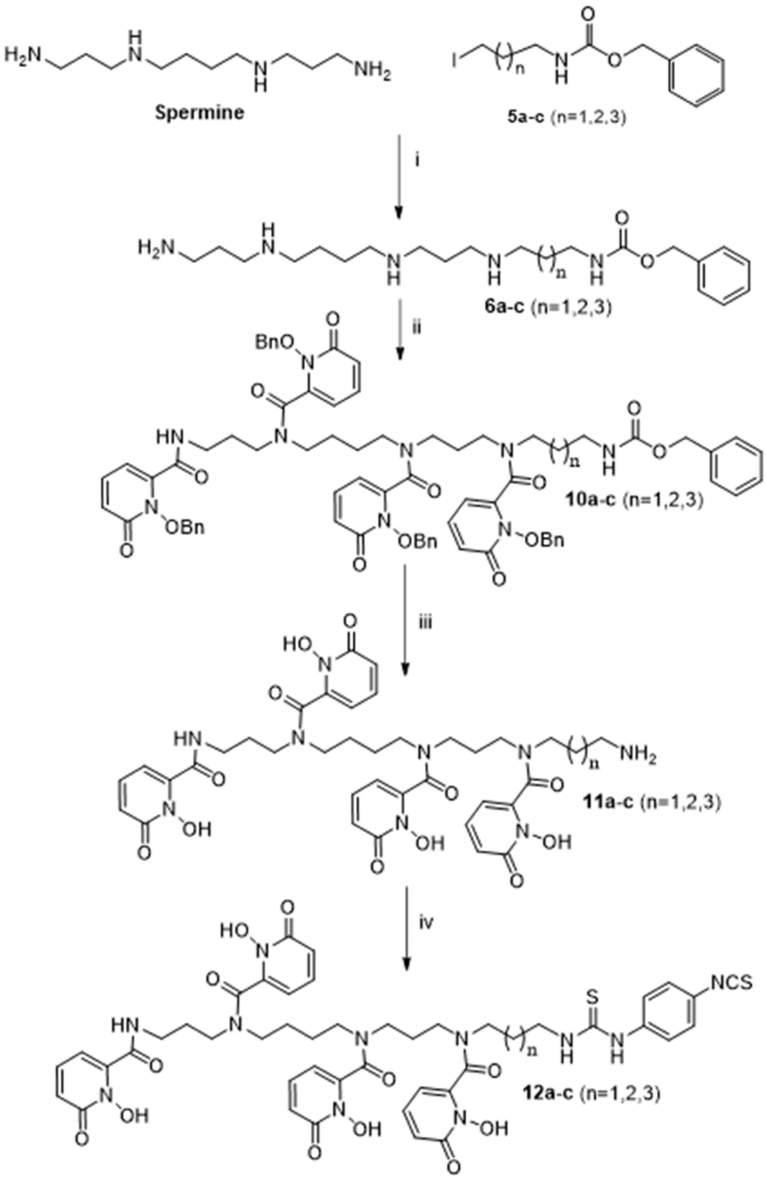

Methods: (i) 3-Benzyloxycarbonyl amino pentane-1-iodide (**5a-c**), Et_3N, ACN, rt, 5h, 76-81%;
(ii) 1-(benzyloxy)-6-oxo-1,6-dihydropyridine-2-carboxylic acid chloride (**9a**), NEt_3, DCM, 0 °C-rt, 1h, 23-24%;
(iii) AcOH:HCl (1:1 v/v), 50 °C, 18 h, 96-97%;
(iv) NEt_3 (excess),IPA/H_2O/$CHCl_3$ (8:2), rt, 2h, 54-55%.

low yield of these *N*-protected amino-alkyl spermine-HOPO derivatives **10a-c** (Scheme S6) was attributed to the formation of mono-HOPO-protected, di-HOPO-protected, and tri-HOPO-protected byproducts. The benzyl and benzyloxy protecting groups were removed by acidic hydrolysis to obtain compounds **11a-c**, (Scheme S7) in a quantitative yield.

The amino-alkyl-spermine-HOPO derivatives **11a-c** were reacted with phenyl-di-isothiocyanate to obtain *p*-SCN-phenyl-alkyl-spermine-HOPO derivatives **12a-c** with up to 55% yields. The final products, *p*-SCN-phenyl-alkyl-spermine-HOPO derivatives **12a-c**, were purified by preparative high-performance liquid chromatography (HPLC) and characterized by ^{1}H NMR, ^{13}C NMR, and high-resolution mass spectrometry (HRMS). The overall yields achieved starting from spermine and alkyl iodide to *p*-SCN-phenyl-alkyl-spermine-HOPO derivatives (**12a-c**, 4 steps, Scheme 1) were 10, 9.8, 10% for **12a**, **12b**, and **12c**, respectively. Compound **13d**, termed *p*-SCN-Bn-C2HOPO (C2HOPO),[46] was synthesized using the synthetic strategy from spermine, with five steps and an overall yield of 3.4% (Scheme 2).

In the literature, Deri et al. initially described a four-step procedure to synthesize a mono-substituted spermine with meager yield, long reaction times, and purification challenges.[46] Bhupathiraju et al. also reported a procedure for mono-substituted spermine formation with low yield (33%); however, they still recovered unreacted spermine and encountered purification issues.[51] Due to the aforementioned purification challenges, results often suffered from poor reactivity issues in subsequent steps. To overcome these issues, this reaction was tested under simpler conditions using 1 equiv of **5a**, which

https://doi.org/10.1021/acsomega.3c01547
ACS Omega 2023, 8, 17181−17194

Scheme 2. : Preparation of *p*-SCN-Bn-C2HOPO (13d) Using the Synthetic Strategy

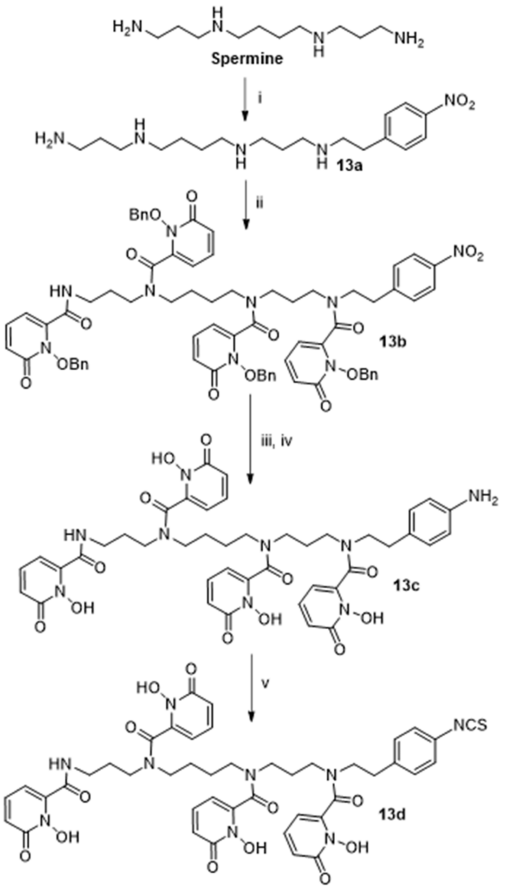

Methods: (i) 4-Nitrophenethyl Bromide, K_2CO_3, DMF, 60 °C, 12 h, 34%;
(ii) 1-(benzyloxy)-6-oxo-1,6-dihydropyridine-2-carboxylic acid chloride, NEt_3, DCM, rt, 2h, 27% (over two steps);
(iii) Raney-Ni, H_2, MeOH:THF, 3h, 52%; (iv) AcOH:HCl (1:1), 50 °C, 18 h, 90%;
(v) 2-di-pyridyl thiocarbonate, NEt_3, ACN:H_2O (8:2), rt, 2h, 54%.

essentially worked as a limiting reagent for the reaction and avoided or limited the formation of undesired products, such as di-, tri-, and tetra-substituted spermine. Because the spermine consisted of two primary amine functionalities at both ends and two secondary amines in the middle of the structure, this provided the opportunity for multi-substitution. By controlling or limiting the addition of **5a** to 1 equiv, spermine as two equivalents using triethylamine as a base, and room temperature for 5 h of reaction time, **6a** was synthesized with 81% yield (Scheme S4). Since spermine was completely consumed in the reaction and the mono-substituted product was very polar due to the presence of the spermine backbone, purification involved simple silica gel column chromatography using a 20%MeOH/10%NH_4OH/70% DCM eluent system, which afforded the pure mono-substituted spermine in high yields.

Deri et al.[46] also demonstrated the superior stability of ^{89}Zr-HOPO compared with ^{89}Zr-DFO and performed the synthesis in nine steps, and Bhupathiraju et al.[51] reported an improved synthesis of *p*-SCN-Bn-HOPO in four major steps. In this study, the chain length of the linker is at one end with three carbons, four carbons, and five carbons without disturbing the functionality of the bifunctional linker. This synthetic strategy provided a facile and more efficient route to synthesize *p*-SCN-Bn-HOPO in four major steps (Scheme 1).[52] Moreover, the design involving HOPO with five carbon chains is similar to that of DFO with five carbon chains, thereby mimicking the linker size in both structures. This increase in carbon chain length for the HOPO analogue design would allow for more steric freedom, ease of conjugation, more flexibility when the ligand was conjugated to either proteins or antibodies, and extended the juxtaposition distance between protein or antibody and ligand.

In summary, we have developed three new HOPO analogues: *p*-SCN-Bn-C3-HOPO (C3HOPO), *p*-SCN-Bn-C4-HOPO (C4HOPO), and *p*-SCN-Bn-C5-HOPO (C5HOPO) utilizing a more efficient synthesis strategy (Table 1). The stability of HOPO analogues was compared to *p*-SCN-Bn-DFO (DFO) as well as their efficacy as chelators for immuno-PET.

***In Vitro* Studies.** First, the stability of novel HOPO ligands (C3-C5HOPO), complexed with ^{89}Zr was determined utilizing a variety of metrics.

EDTA Challenge Test. Foremost, the stability of C3-C5HOPO, C2HOPO, and DFO ligands (free chelates) radiolabeled with ^{89}Zr was tested in the presence of EDTA. To do so, the free chelates were radiolabeled with ^{89}Zr under mild conditions, pH 7 at room temperature. DFO chelator labeled within 1 h and HOPO derivates labeled within 2 h. Labeling efficiency was quantified by radio-TLC and labeled chelates were purified using a PD-10 column. To evaluate the stability of the ^{89}Zr-ligand complexes, complexes were incubated with a 10-fold excess of ethylenediamine tetraacetic acid (EDTA) at pH 5, 6, 7, and 8, at 37 °C for 7 days. Subsequently, the stability of the complexes was monitored by radio-TLC every 24 h for 7 days post initial incubation. The ^{89}Zr-C3-C5HOPO and ^{89}Zr-C2HOPO complexes remained intact (>99.5%) throughout the 7-day testing period and retained stability at each pH (Table 2). In contrast, ^{89}Zr-DFO complexes were extremely unstable and demonstrated a high percent transchelation, especially at pH 5.0 (Table 2). Thus, the ^{89}Zr-C3-C5HOPO complexes demonstrated excellent stability during an ETDA challenge test, comparable to the stability of the ^{89}Zr-C2HOPO complex, and with significantly better stability compared to the ^{89}Zr-DFO complexes.

Thermal Stability. Next, the thermal stability of the HOPO and DFO ^{89}Zr-labeled complexes was tested when HOPO and DFO chelates were conjugated to a biologically relevant protein, BSA. DFO, C3HOPO, C4HOPO, C5HOPO, and C2HOPO derivatives were conjugated to BSA through a thiourea moiety, where the isothiocyanate functional group of the DFO or HOPO derivative reacted with the amine functional group of lysine residues. BSA conjugates were subsequently purified using dialysis cassettes. BSA conjugates were radiolabeled with ^{89}Zr utilizing the same conditions as when radiolabeling the free chelates. Radio chemical yields (n = 2 labelings) were 82, 95, 89, 90, and 98% for DFO, C2-HOPO, C3-HOPO, C4-HOPO, and C5-HOPO, respectively. Molar activity (n = 2 labelings; Bq/mol) were 8×10^{15}, 6×10^{15}, 7×10^{15}, 7×10^{15}, and 5×10^{15} for DFO, C2-HOPO, C3-HOPO, C4-HOPO, and C5-HOPO, respectively. Subsequently, they were incubated in PBS at 4 °C, room temperature, and 37 °C, and stability was monitored by radio-TLC at 24 and 48 h. Similar to the EDTA challenge, ^{89}Zr-C3-C5HOPO-BSAs and ^{89}Zr-C2HOPO-BSA complexes demonstrated high thermal stability, while ^{89}Zr-DFO-BSA was less stable at each temperature over time (Table S2).

pH Stability. The pH stability of the chelators was tested when conjugated to monoclonal anti-PD- L1 antibodies (STM004 and STM108) at 37 °C. After testing the conjugation efficiency of all of the HOPO analogues, C5HOPO derivative

https://doi.org/10.1021/acsomega.3c01547
ACS Omega 2023, 8, 17181−17194

Table 1. Summary of HOPO Analogues Compared to DFO[a]

Chelator Nomenclature	Chelator Structure
N1-hydroxy-N1-(5-(4-(hydroxy(5-(3-(4-isothiocyanatophenyl)thioureido)pentyl)amino)-4-oxobutanamido)pentyl)-N4-(5-(N-hydroxyacetamido)pentyl)succinamide (**p-SCN-Bn-DFO**)	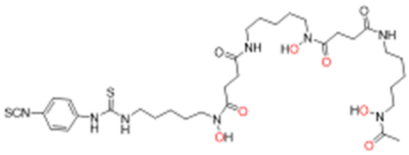
1-hydroxy-N-(3-(1-hydroxy-6-oxo-1,6-dihydropyridine-2-carboxamido)propyl)-N-(4-(1-hydroxy-N-(3-(1-hydroxy-N-(3-(3-(4-isothiocyanatophenyl)thioureido)propyl)-6-oxo-1,6-dihydropyridine-2-carboxamido)propyl)-6-oxo-1,6-dihydropyridine-2-carboxamido)butyl)-6-oxo-1,6-dihydropyridine-2-carboxamide (**p-SCN-Bn-C3HOPO**)	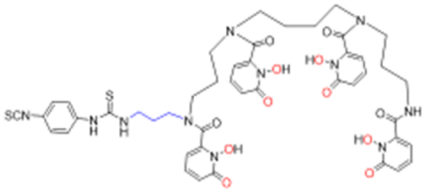
1-hydroxy-N-(3-(1-hydroxy-6-oxo-1,6-dihydropyridine-2-carboxamido)propyl)-N-(4-(1-hydroxy-N-(3-(1-hydroxy-N-(4-(3-(4-isothiocyanatophenyl)thioureido)butyl)-6-oxo-1,6-dihydropyridine-2-carboxamido)propyl)-6-oxo-1,6-dihydropyridine-2-carboxamido)butyl)-6-oxo-1,6-dihydropyridine-2-carboxamide (**p-SCN-Bn-C4HOPO**)	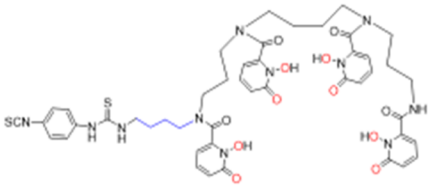
1-hydroxy-N-(3-(1-hydroxy-6-oxo-1,6-dihydropyridine-2-carboxamido)propyl)-N-(4-(1-hydroxy-N-(3-(1-hydroxy-N-(5-(3-(4-isothiocyanatophenyl)thioureido)pentyl)-6-oxo-1,6-dihydropyridine-2-carboxamido)propyl)-6-oxo-1,6-dihydropyridine-2-carboxamido)butyl)-6-oxo-1,6-dihydropyridine-2-carboxamide (**p-SCN-Bn-C5HOPO**)	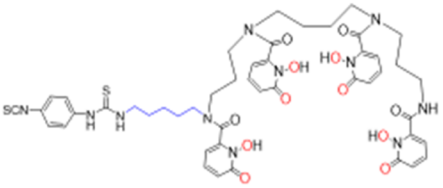

[a]Three new HOPO analogues were synthesized: *p*-SCN-Bn-C3HOPO (C3HOPO), *p*-SCN-Bn-C4HOPO (C4HOPO), and *p*-SCN-Bn-C5HOPO (C5HOPO). In this table, the nomenclature and structure of each chelator are described and how they compare to *p*-SCN-Bn-DFO (DFO).

Table 2. EDTA Challenge Study of ^{89}Zr-DFO, ^{89}Zr-C3HOPO, ^{89}Zr-C4HOPO, ^{89}Zr-C5HOPO, and ^{89}Zr-C2HOPO with BSA Protein[a]

Chelate	pH	Initial	1 d	2 d	3 d	4 d	5 d	6 d	7 d
^{89}Zr-DFO	5	99.9	2.3±0.7	0.8±0.2	0.8±0.1	0.1±0.9	0.0	0.0	0.0
	6	99.9	15.3±3.1	2.1±0.4	1.8±0.3	1.5±0.1	1.4±0.1	1.3±0.0	1.3±0.1
	7	99.9	22.0±2.2	13.7±1.8	12.9±1.0	12.7±0.7	12.6±0.5	11.7±0.4	11.2±0.5
	8	99.9	98.4±0.7	98.0±1.2	98.1±0.8	92.1±0.5	89.4±0.7	75.2±0.7	74.4±0.4
^{89}Zr-C3HOPO	5	100	100.0	100.0	100.0	100.0	100.0	100.0	100.0
	6	100.0	100.0	100.0	100.0	100.0	100.0	100.0	100.0
	7	100.0	100.0	100.0	100.0	100.0	100.0	100.0	100.0
	8	100.0	100.0	100.0	100.0	100.0	100.0	100.0	100.0
^{89}Zr-C4HOPO	5	100.0	100.0	100.0	100.0	100.0	100.0	100.0	100.0
	6	100.0	100.0	100.0	100.0	100.0	100.0	100.0	100.0
	7	100.0	100.0	100.0	100.0	100.0	100.0	100.0	100.0
	8	100.0	100.0	100.0	100.0	100.0	100.0	100.0	100.0
^{89}Zr-C5HOPO	5	100.0	100.0	100.0	100.0	100.0	100.0	100.0	100.0
	6	100.0	100.0	100.0	100.0	100.0	100.0	100.0	100.0
	7	100.0	100.0	100.0	100.0	100.0	100.0	100.0	100.0
	8	100.0	100.0	100.0	100.0	100.0	100.0	100.0	100.0
^{89}Zr-C2HOPO	5	100.0	100.0	100.0	100.0	100.0	100.0	100	100.0
	6	100.0	100.0	100.0	100.0	100.0	100.0	100	100.0
	7	100.0	100.0	100.0	100.0	100.0	100.0	100.0	100.0
	8	100.0	100.0	100.0	100.0	100.0	100.0	100.0	100.0

[a]Data are mean% values ± standard deviation of their initial value (n = 3). Green color indicates the stability of ^{89}Zr-labeled complexes >99% intact. Yellow indicates 90−99%, orange indicates 70−90%, and red indicates <70% (unstable).

https://doi.org/10.1021/acsomega.3c01547
ACS Omega 2023, 8, 17181−17194

Table 3. pH Stability of ^{89}Zr-DFO-STM004, ^{89}Zr-DFO-STM108, ^{89}Zr-C5HOPO-STM004, and ^{89}Zr-C5HOPO-STM108 at Physiologic pH (7) at 37 °C[a]

Antibody conjugate	pH	Initial	1 d	2 d	3 d	4 d	5 d	6 d	7 d
^{89}Zr-DFO-STM004	7	99.9	99.3±0.8	91.4±2.9	84.8±7.9	82.4±6.7	81.7±5.5	79.6±2.4	74.3±6.4
^{89}Zr-DFO-STM108	7	100	92.9±5.5	81.7±2.6	69.0±5.7	68.4±5.2	66.5±4.5	64.3±5.4	62.6±3.1
^{89}Zr-C5 HOPO-STM004	7	99.9±0.05	99.9±0.0	99.9±0.0	99.9±0.0	99.9±0.0	99.9±0.0	99.9±0.0	99.9±0.0
^{89}Zr-C5 HOPO-STM108	7	99.9±0.05	99.9±0.0	99.9±0.0	99.9±0.0	99.9±0.0	99.9±0.0	99.9±0.0	99.9±0.0

[a]Green color indicates stability of ^{89}Zr-labeled complexes >99% intact. Yellow indicates 90−99%, orange indicates 70−90%, and red indicates <70% (unstable).

Table 4. Serum Stability of ^{89}Zr-DFO-STM004, ^{89}Zr-DFO-STM108, ^{89}Zr-HOPO-STM004, and ^{89}Zr-HOPO-STM108 Complexes[a]

	Human serum				Mouse serum			
	Initial (%)	24 h	48 h	72 h	Initial (%)	24 h	48 h	72 h
^{89}Zr-DFO-BSA	99.9±0.0	6.3±4.7	4.6±3.1	3.8±2.9	99.9±0.0	23.5±16.8	12.1±2.7	10.7±2.2
^{89}Zr-C5HOPO-BSA	100	99.9±0.0	99.9±0.0	99.9±0.0	100	99.99±0.0	99.98±0.0	99.96±0.0
^{89}Zr-DFO-STM004	99.9±0.0	41.6±4.0	37.6±2.0	28.0±3.6	99.9±0.0	29.6±8.0	29.3±8.0	20.3±4.5
^{89}Zr-DFO-STM108	100	89.2±1.7	81.9±5.2	78.0±5.1	100	76.0±1.7	39.5±4.2	32.3±3.0
^{89}Zr-C5HOPO-STM004	99.9±0.0	99.1±0.5	99.0±0.5	99.1±0.2	99.9±0.0	99.3±0.2	98.7±0.5	98.7±0.5
^{89}Zr-C5HOPO-STM108	100.0±0.0	99.2±0.5	99.1±0.3	99.9±0.0	100.0±0.0	99.8±0.0	99.5±0.5	99.8±0.0

[a]Data are mean% values ± standard deviations of their initial values (n = 3). Green color indicates the stability of ^{89}Zr-labeled complexes >99% intact. Yellow indicates 90−99%, orange indicates 70−90%, and red indicates <70%.

proved to be the easiest to conjugate, and thus, this derivative was selected for further evaluating new HOPO analogues conjugated to monoclonal antibodies. Both DFO and C5HOPO were conjugated to the monoclonal antibodies STM004 and STM108 using a ligand-to-antibody ratio of 5:1 (DFO) and 15:1 (C5HOPO derivative) and subsequently purified using dialysis cassettes. The 15:1 ligand-to-antibody conjugation ratio was chosen when conjugating C5HOPO because the 5:1 ligand-to-antibody conjugation ratio proved unsuccessful. To determine the maximum molar activities of each HOPO-antibody, the starting volume of each HOPO-antibody was varied. 30 μL of starting antibody yielded 20−39% labeling efficiency, and 60 μL was sufficient to achieve maximum molar activity. DFO- and C5HOPO-conjugated STM004 and STM108 were radiolabeled with ^{89}Zr, as described in Figures S1−S8 and Table S1. ^{89}Zr-C5HOPO-STM004 was obtained in a radiochemical yield of 52 ± 4% (n = 6), and ^{89}Zr-C5HOPO-STM108 was obtained in only 6.5 ± 1.5% (n = 6) radiochemical yield, with a molar activity of 9.4 ± 1.6 × 10^{15} Bq/mol. Poor radiolabeling of STM108 may be attributed to a less efficient conjugation of bifunctional chelator to the antibody, antibody aggregation,[53] radiolysis, and/or insufficient removal of hydrolyzed p-NCS-Bn-C5HOPO after conjugation.

The pH stability of ^{89}Zr-DFO-STM004, ^{89}Zr-DFO-STM108, ^{89}Zr-C5HOPO-STM004, and ^{89}Zr-C5HOPO-STM108 was evaluated at 37 °C in PBS at pH 5, 6, 7, and 8 over 7 days by radio-TLC. ^{89}Zr-DFO-STM004 showed significant instability (34%) at pH 5.0 and moderate stability (65 to 76%) as the pH increased from 6 to 8 (Table 3 (pH 7) and Table S3 (pH 5, 6, and 8)). In contrast, both ^{89}Zr-C5HOPO antibodies remained highly stable at 37 °C in PBS at pH 5, 6, and 7, with only a minimal decrease in stability at pH 8 (up to 90% ± 3.0) (Table 3 (pH 7) and Table S3 (pH 5, 6, and 8)).

The stabilities of ^{89}Zr-DFO and ^{89}Zr-C5HOPO were further compared. Stability was tested with BSA conjugates, STM004 or STM108 monoclonal antibodies conjugates at 48 h at physiological pH. The percent stability of conjugated ^{89}Zr-C5HOPO-BSA protein was 6.7 percentage points higher than ^{89}Zr-DFO-BSA (Figure S9). Similarly, when comparing the percent stabilities of the ^{89}Zr labeled complexes conjugated to monoclonal antibodies, the stability of ^{89}Zr-C5HOPO-STM004 was 28 percentage points higher than ^{89}Zr-DFO-STM004, and the critical antibody ^{89}Zr-C5HOPO-STM108 was 18 percentage points higher than ^{89}Zr-DFO-STM108 (Figure S9). These results indicated that ^{89}Zr-labeled C5HOPO were significantly (p < 0.0001, 2-way ANOVA, column factor DFO vs HOPO) more stable *in vitro* than their corresponding ^{89}Zr-labeled DFO congeners.

Serum Stability. Next, the serum stability of ^{89}Zr-DFO-BSA and ^{89}Zr-C5HOPO-BSA complexes in both human serum and mouse serum at 37 °C for up to 72 h was tested and compared. The serum stability of the ^{89}Zr-DFO-BSA and ^{89}Zr-C5HOPO-BSA complexes was monitored by radio-TLC every 24 h for up to 72 h post-incubation. ^{89}Zr-DFO-BSA was extremely unstable at 72 h (3.8% ± 2.92) compared to its initial value in human serum and similarly unstable (10.7% ± 2.20 at 72 h) in mouse serum (Table 4). This instability was due to the de-chelation of ^{89}Zr from DFO. In contrast, the ^{89}Zr-C5HOPO-BSA complex was extremely stable (>99.5% at 72 h) in both human and mouse serum (Table 4).

Next, the stability of ^{89}Zr-labeled C5HOPO and DFO when conjugated to monoclonal antibodies STM004 and STM108 in both human serum and mouse serum was evaluated. Similar to when the chelators were conjugated to BSA, the stability of ^{89}Zr-DFO-STM004 diminished significantly at 72 h to 28.0% ± 3.60 in human serum and 20.3% ± 4.50 in mouse serum (Table 4). After 72 h, ^{89}Zr-DFO-STM108 was stable in human serum

https://doi.org/10.1021/acsomega.3c01547
ACS Omega 2023, 8, 17181−17194

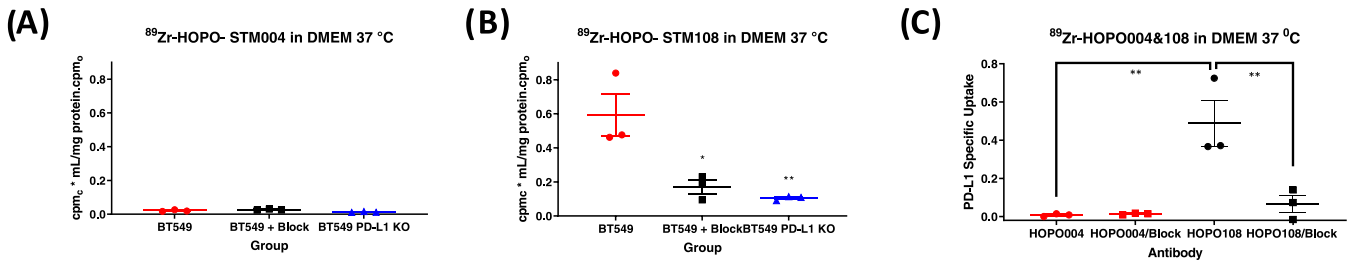

Figure 2. Live cell binding assays of ^{89}Zr-C5HOPO-STM004 (A) and ^{89}Zr-C5HOPO-STM108 (B) in DMEM at 37 °C. Comparative PD-L1 specific binding (binding of blocked or unblocked for the respective labeled antibody minus binding of KO cell line for the respective labeled antibody) of ^{89}Zr-C5HOPO-STM004 or ^{89}Zr-C5HOPO-STM108 in DMEM at 37 °C (C). Data are mean ± standard deviation (n = 3); KO, PD-L1 knockout; $^{**}p \leq 0.01$, $^{*}p \leq 0.05$.

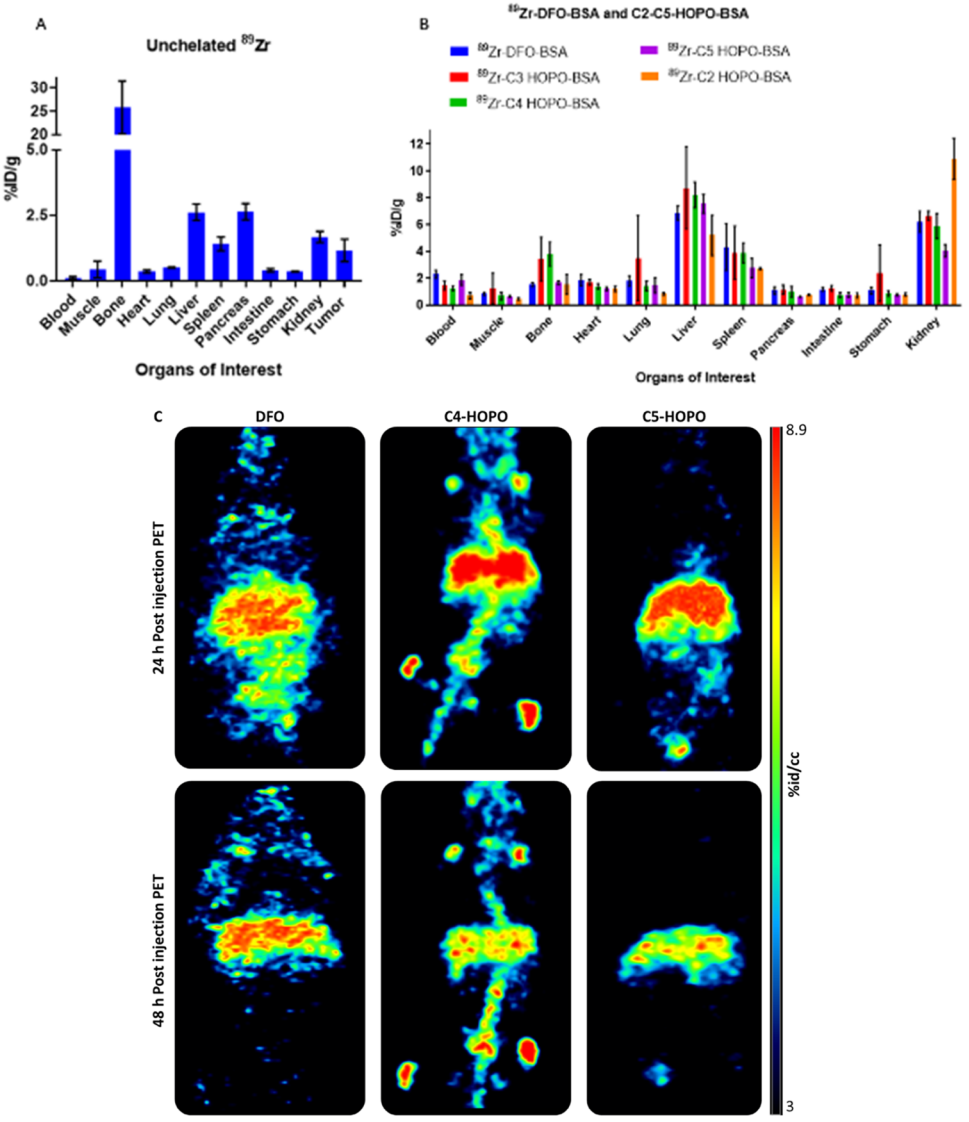

Figure 3. (A) Biodistribution of free or unchelated ^{89}Zr at 144 h after injection of four mice bearing BT549 tumor xenografts. (B) Comparative biodistribution of ^{89}Zr-DFO-BSA, ^{89}Zr-C3-C5HOPO-BSA, and ^{89}Zr-C2HOPO-BSA (48 h post-injection, n = 4 for each labeled protein) in healthy female athymic nude mice. Data are mean %ID/g value ± standard deviation. %ID/g, percent injected dose per gram. (C) Representative PET coronal maximum intensity projections of ^{89}Zr-labeled-BSA: ^{89}Zr-DFO-BSA, ^{89}Zr-C4-HOPO-BSA, ^{89}Zr-C5-HOPO-BSA at 24 and 48 h post-injection.

(78.0% ± 5.19) but proved unstable in mouse serum (32.3% ± 3.05) (Table 4).

In contrast, ^{89}Zr-C5HOPO-STM004 and ^{89}Zr-C5HOPO-STM108 were highly stable in human serum (99.1% ± 0.23, 99.9% ± 0.05) and mouse serum (98.7% ± 0.58, 99.8% ± 0.05) at 72 h, respectively (Table 4). These results further demonstrated the high stability of ^{89}Zr-labeled C5HOPO when conjugated to BSA or monoclonal antibodies (STM004 and STM108) in mouse and human serum.

https://doi.org/10.1021/acsomega.3c01547
ACS Omega 2023, 8, 17181−17194

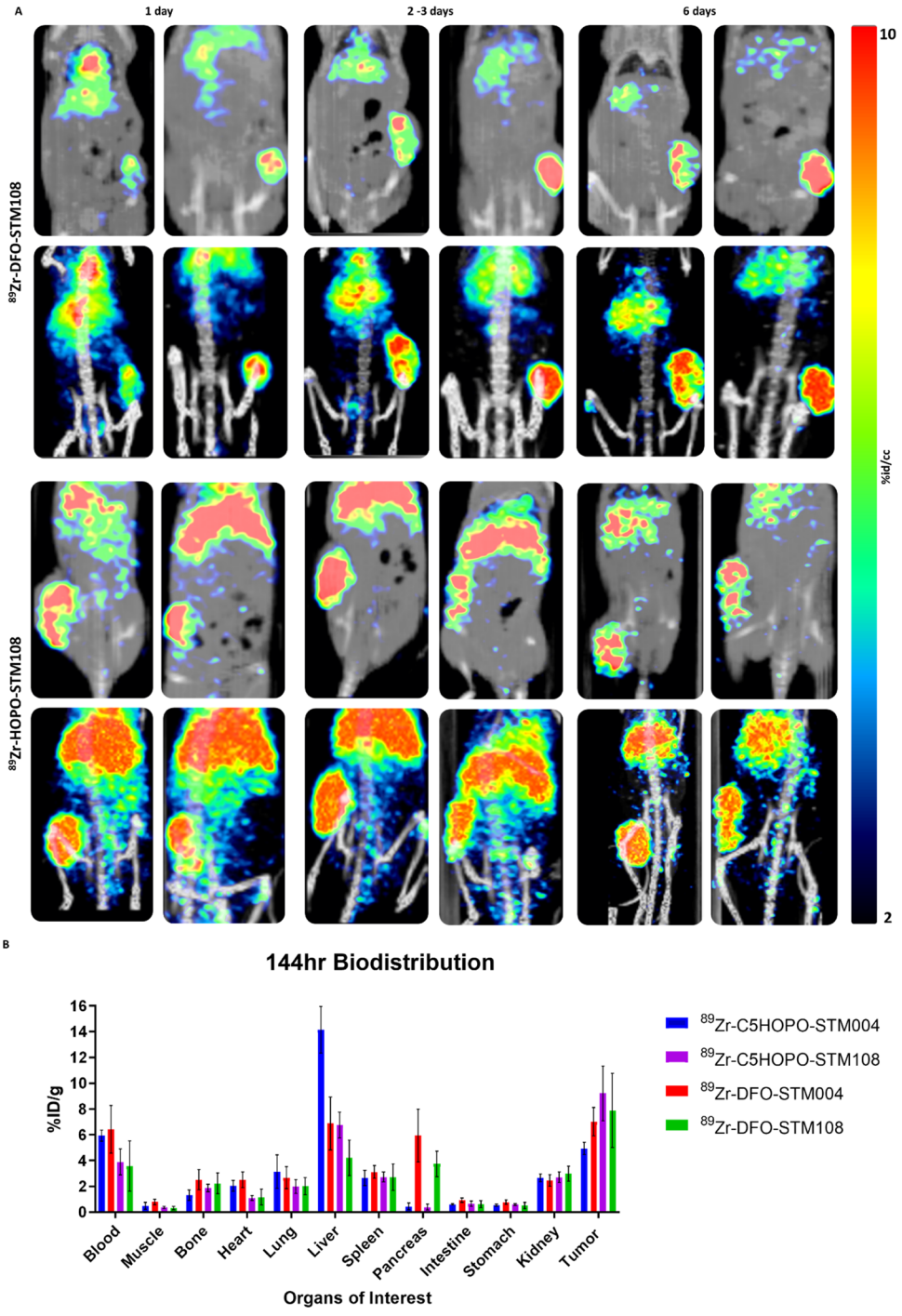

Figure 4. (A) PET/CT imaging *in vivo* of ^{89}Zr-DFO-STM108 and ^{89}Zr-C5HOPO-STM108 at 1 day, 2−3 days, and 6 days post-injection (coronal images at the top and coronal maximum intensity projection images at the bottom for each antibody) in mice with BT549 tumor xenografts. %ID/cc, percent injected dose/cubic centimeter. Two exemplar mice were provided per group. (B) Biodistribution of ^{89}Zr-C5HOPO-STM004 (n = 4), ^{89}Zr-C5HOPO-STM108 (n = 4), ^{89}Zr-DFO-STM004 (n = 4), and ^{89}Zr-DFO-STM108 (n = 4) at 144 h after injection in mice bearing BT549 tumor xenografts. Data are mean%ID/g value ± standard deviation. %ID/g, percent injected dose per gram.

Live Cell Binding Assay. After demonstrating that ^{89}Zr-C5HOPO has high stability by several metrics *in vitro*, C5HOPO was evaluated as new chelator for immuno-PET. As an exemplar application, imaging PD-L1 was selected. Two anti-PD-L1 antibodies with relatively high (STM108) and low (STM004) affinity for PD-L1 were selected for evaluation.[50] First, live cell binding and blocking experiments were conducted in order to confirm that STM004 and STM108, when conjugated to C5HOPO, retained PD-L1 binding and expected rank order of cell retention. BT549 cells, a high PD-L1 expressing human TNBC cell line, or BT549 PD-L1 KO cells were incubated with ^{89}Zr-C5HOPO-STM004 or ^{89}Zr-C5HOPO-STM108. For blocking experiments, excess of the corresponding cold antibodies (STM004 and STM108, 50×) was added 20 min before the addition of the labeled antibodies. Cells were incubated with the labeled antibodies for 60 min at 37 °C, washed three times with ice-cold DMEM, and cell-associated activity was assessed by a γ counter and protein

https://doi.org/10.1021/acsomega.3c01547
ACS Omega 2023, 8, 17181−17194

Table 5. Biodistribution *In Vivo* (%ID/g)[a]

organ	^{89}Zr-DFO-STM004	^{89}Zr-HOPO-STM004	^{89}Zr-DFO-STM108	^{89}Zr-HOPO-STM108	*p*-value
blood	6.4 ± 1.8	5.9 ± 0.4	3.5 ± 1.9	3.9 ± 1.0	0.778518
muscle	0.8 ± 0.2	0.5 ± 0.2	0.3 ± 0.1	0.3 ± 0.0	0.527813
bone	2.5 ± 0.7	1.3 ± 0.4	2.2 ± 0.8	1.8 ± 0.2	0.442526
heart	2.5 ± 0.6	2.0 ± 0.4	1.1 ± 0.6	1.1 ± 0.1	0.821979
lung	2.6 ± 0.8	3.1 ± 1.2	2.0 ± 0.6	2.0 ± 0.5	0.981605
liver	6.8 ± 2.0	14.1 ± 1.8	4.2 ± 1.3	6.7 ± 0.9	0.023795
spleen	3.1 ± 0.4	2.6 ± 0.5	2.7 ± 1.0	2.7 ± 0.3	0.990775
pancreas	5.9 ± 2.0	0.4 ± 0.2	3.7 ± 0.9	0.4 ± 0.2	0.00057
intestine	0.9 ± 0.1	0.6 ± 0.0	0.6 ± 0.2	0.6 ± 0.1	0.795714
stomach	0.7 ± 0.1	0.5 ± 0.0	0.5 ± 0.2	0.6 ± 0.0	0.615244
kidney	2.4 ± 0.4	2.6 ± 0.3	2.9 ± 0.5	2.6 ± 0.4	0.461984
tumor	7.0 ± 1.1	4.9 ± 0.4	7.8 ± 2.8	9.2 ± 2.1	0.484761

[a]Biodistribution data of ^{89}Zr-labeled DFO- and HOPO-anti-PD-L1 antibodies at 144 h after injection. Data are mean%ID/g value ± standard deviation (n = 4). Results of unpaired t-tests of the respective ROI organ data comparing ^{89}Zr-DFO-STM108 vs ^{89}Zr-HOPO-STM108 are shown (p-values). Adjusted acceptance level should be $p < 0.004$ when adjusted for multiple tests.

mass by BCA assay. ^{89}Zr-C5HOPO-STM004 showed relatively low binding to BT549 WT cells (0.021 ± 0.005 cpm_c·mL/mg protein·cpm_o) (Figure 2A), which was slightly diminished in BT549 PD-L1 KO cells (0.013 ± 0.002 cpm_c·mL/mg protein·cpm_o) and was minimally displaced by cold STM004. Conversely, ^{89}Zr-C5HOPO-STM108 demonstrated relatively high cell binding to BT549 WT cells (0.59 ± 0.21 cpm_c·mL/mg protein·cpm_o), which was significantly diminished in BT549 PD-L1 KO cells (0.10 ± 0.01 cpm_c·mL/mg protein·cpm_o) and displaceable by ∼10-fold with cold STM108, confirming the binding and specificity of ^{89}Zr-C5HOPO-STM108 to PD-L1 (Figure 2B) and the expected rank order from the prior literature. These results demonstrated that ^{89}Zr-labeled C5HOPO-conjugated anti-PD-L1 antibodies reflected the known binding and specificity for PD-L1 of the native antibodies[50] (Figure 2C). Similar results were also obtained when cells were incubated with ^{89}Zr-labeled DFO-conjugated anti-PD-L1 antibodies or incubated in MEBSS solution (Figures S10 and S11). Rank order specificity was confirmed by fluorescence microscopy. There was more specific binding of STM108 by PD-L1 expressing cells compared to STM004 both by the antibodies alone or when conjugated to C5HOPO or DFO (Figure S12).

In Vivo Studies. Next, C5HOPO was evaluated as a new chelator for immuno-PET by testing the binding and retention of ^{89}Zr-labeled anti-PD-L1 antibodies in mice harboring TNBC BT549 tumors, the same cancer cells utilized for studies *in vitro*. Prior to injecting ^{89}Zr-labeled C5HOPO PD-L1 antibodies into mice bearing BT549 tumor xenografts, we assessed the behavior *in vivo* of free or unchelated ^{89}Zr. ^{89}Zr was neutralized, passed through a PD-10 column, eluted with PBS, and injected into tumor-bearing mice (n = 4), which were then imaged by PET/CT. The resulting biodistribution demonstrated high uptake of free ^{89}Zr in the bone (25.76 ± 5.46% ID/g) (Figure 3A). This served as a control for free $^{89}Zr^{4+}$, generally known to accumulate in the bone. The liver and kidney showed much less retention than did the bone, and there was little specific binding in the tumor.

Next, the overall biodistribution of C5HOPO was compared to other chelators when conjugated to a nontargeted protein, BSA. Healthy female athymic nude mice (n = 4 for each labeled protein) were injected with ^{89}Zr-DFO-BSA, ^{89}Zr-C3-C5HOPO-BSA, or ^{89}Zr-C2HOPO-BSA, and mice were imaged at 24 and 48 h by PET. The animals were humanely euthanized after the 48 h PET scans. Organs were isolated and weighed, and radioactivity was counted using a γ counter. The percent injected dose per gram (% ID/g) was calculated (mean ± standard deviation) for all labeled BSA conjugates. Comparative biodistribution studies of ^{89}Zr-DFO-BSA, ^{89}Zr-C3-C5HOPO-BSA, and ^{89}Zr-C2HOPO-BSA at 48 h post-injection found only slight retention differences. Most of the activity accumulated in the liver and slowly cleared through the kidney (Figure 3B). Overall, once chelated, across all labeled proteins, there was minimal bone uptake compared to the high bone uptake seen with free ^{89}Zr. ^{89}Zr-DFO-BSA and ^{89}Zr-C5HOPO-BSA showed the lowest bone uptake of 1.55 ± 0.15 and 1.68 ± 0.13% ID/g at 48 h, respectively. These results further demonstrated the high stability of C5HOPO *in vivo* (Figure 3B,C).

Next, the tumor-targeting capacities of ^{89}Zr-labeled C5HOPO-conjugated anti-PD-L1 antibodies were characterized using the high PD-L1 expressing BT-549 TNBC model. 5×10^6 BT-549 cells were implanted by subcutaneous injection into the right flank of 5-week-old female athymic nude mice. Tumor growth was monitored until tumors reached a minimal volume of 100−150 mm^3 (Figures S13 and S14). The mice were injected with ^{89}Zr-labeled-anti-PD-L1 antibodies through tail vein IV injection (approx. 12−15 μCi/mouse) under anesthesia and PET/CT scans were performed at 24, 48, and 144 h after injection of the labeled antibodies. Biodistribution studies *ex vivo* were carried out on all of the animals after PET/CT imaging at 144 h.

Both ^{89}Zr-labeled C5HOPO-STM108 and C5HOPO-STM004 demonstrated good overall tumor targeting by PET/CT (Figures 4 and S16). Biodistribution data demonstrated that ^{89}Zr-C5HOPO-STM108 showed higher tumor accumulation (9.21 ± 2.12% ID/g) compared to ^{89}Zr-C5HOPO-STM004 (4.94 ± 0.46% ID/g) and lower overall liver accumulation, 6.7 ± 0.9% ID/g compared to 14.1 ± 1.8% ID/g, respectively (Figures 4 and S16 and Table 5). In addition, ^{89}Zr-C5HOPO-STM108 had a more favorable tumor-to-blood ratio than ^{89}Zr-C5HOPO-STM004 at 144 h: 2.36 compared to 0.83, respectively; tumor-to-liver ratio, 1.37 compared to 0.35, respectively; and tumor-to-muscle ratio 30.6 compared to 9.8, respectively. These data demonstrated that C5HOPO could perform as an excellent chelator for immuno-PET. In addition, the better overall performance of ^{89}Zr-C5HOPO-STM108 compared to ^{89}Zr-C5HOPO-STM004 for *in vivo* imaging of PD-L1 was likely reflective of the higher overall affinity of STM108 for PD-L1

https://doi.org/10.1021/acsomega.3c01547
ACS Omega 2023, 8, 17181−17194

compared to STM004. Similar results were also obtained when DFO was used (Figures 4 and S16 and Table 5). In addition, both ^{89}Zr-C5HOPO-STM108 and ^{89}Zr-C5HOPO-STM004 demonstrated a trend toward lower overall bone uptake compared to ^{89}Zr-DFO-STM108 and ^{89}Zr-DFO-STM004 *in vivo* (Figure 4B) as also seen with ^{89}Zr-C5HOPO-BSA versus ^{89}Zr-DFO-BSA (Figure S15), but not reaching statistical significance.

DISCUSSION

In summary, an improved synthesis was developed for the production and testing of *p*-SCN-phenyl-alkyl-spermine-HOPO with three different carbon chain lengths (C3, C4, and C5) in four major steps with 9.8 ± 0.2% overall yields. Thermal and serum stability assessments demonstrated that the new HOPO derivatives were significantly more stable *in vitro* compared to DFO. Furthermore, when C5HOPO was utilized as a chelator for immuno-PET using two anti-PD-L1 antibodies, STM108 and STM004, ^{89}Zr-C5HOPO-STM108 and ^{89}Zr-C5HOPO-STM004 demonstrated high tumor binding in PD-L1 expressing BT-594 xenografts and low overall bone uptake. Relative tumor binding in this model was also reflective of the native affinity differences of STM108 and STM004 for PD-L1, respectively.

These results are similar to those that compared the stability of DFO to DFO* and DFOcyclo* conjugated to trastuzumab, wherein it was found that DFO-trastuzumab was very unstable *in vitro* and that stability *in vitro* of DFO*-trastuzumab and DFOcyclo*-trastuzumab were significantly improved. Similar to HOPO, both DFO* and DFOcyclo* have additional coordinating oxygen moieties compared to DFO, allowing for greater stability *in vitro*,[45] similar to C5HOPO. However, when bone retention of ^{89}Zr-labeled C5HOPO-anti-PD-L1 was compared to ^{89}Zr-labeled DFO-anti-PD-L1, only minor differences in overall biodistribution and tumor-specific binding between labeled products were observed. In addition, regardless of *in vitro* stability, all radiolabeled proteins demonstrated little bone uptake and thus proved to be highly stable *in vivo*. Recently, Sharma et al. demonstrated that bone retention *in vivo* of ^{89}Zr-DFO antibodies was highly dependent on the FcγR-mediated binding of antibodies by myeloid cells, which have high FcγR expression, and among other locations, reside in the bone marrow. They also demonstrated that the immunodeficiency status of the mice used in these experiments, which dictates the levels of FcγR-expressing myeloid cells, directly affects the amount of bone uptake and subsequent biodistribution of different radiolabeled antibodies observed *in vivo*.[54] Additionally, antibody isotype and CDR occupancy also dictate FcγR affinity and, because many chelator conjugation strategies are not site-specific and the Fc fragment is the dominant site for chelator attachment, chelator conjugate sites may also differentially affect FcγR affinity of different antibodies.[55,56] Thus, variation in mice strains and antibodies utilized in different experiments may have a direct affect on the variability of bone retention and therefore inferred stability *in vivo* between different radiolabeled proteins in different experiments. As such, we postulate that although the number of oxygen coordinators of the chelator is the dominant factor affecting *in vitro* stability, antibody isotype, chelator location on the Fc fragment, and engagement with FcγR on myeloid cells are the dominant factors affecting stability *in vivo*. However, although interactions with FcγRs likely dominate the apparent stability *in vivo* of radiolabeled antibodies, in certain contexts and disease states, the additional stability afforded by chelators such as C5HOPO with additional coordinating oxygen donors may still be beneficial and add additional improved stability over other chelators such as DFO.

Overall, the results suggested that ^{89}Zr-labeled C5HOPO-STM108 was a robust candidate PET imaging agent for assessing disease progression and treatment monitoring of immunotherapy due to its significant PD-L1-specific binding *in vitro* and significant tumor binding *in vivo*. Furthermore, C5HOPO was demonstrated to be a high-quality chelator for PD-L1 PET imaging owing to its ease of synthesis and stability with significant potential for future applications.

EXPERIMENTAL PROCEDURES

Materials, Methods, and Synthesis Details. Synthesis of all starting materials, intermediates, and precursors, as well as their characterization are included in the Supporting Information.

EDTA Challenge Study. This study was performed according to a previously published procedure.[35] After radiolabeling of HOPO and DFO ligands with ^{89}Zr, an initial measurement of the percentage of labeling was made using radio-TLC. Next, 275 μL of samples was prepared, consisting of 25 μL of ^{89}Zr solution (~50 μCi) at pH 7, 200 μL of 5 mM EDTA at different pH levels (5, 6, 7, and 8), and 50 μL of 1 M ammonium acetate at different pH levels (5, 6, 7, and 8) added to maintain the required pH for the duration of the experiment. All samples were incubated in a heat block at 37 °C for 7 days with occasional shaking. The stability of the samples was monitored by radio-TLC every 24 h for up to 7 days post-incubation. Each sample was then spotted onto an ITLC strip, developed in the mobile phase, and analyzed to obtain the percentage of stable labeling. Samples were prepared at each pH in triplicate.

Conjugation Experiments. *Conjugation of Chelators to BSA.* Two cassettes were soaked in 0.1 M $NaHCO_3$ (350 mL) for 10 min. Next, 900 μL of 1% BSA in PBS was diluted with 600 μL of 0.1 M $NaHCO_3$ as a stock solution. Then, 500 μL was injected into each of two cassettes and placed in two separate beakers containing 350 mL of 0.1 M $NaHCO_3$ each. The cassettes were rotated for 3 h. After 3 h, 0.1 M $NaHCO_3$ buffer was replaced twice. Cassettes were removed, and 1% BSA in PBS was recovered into an Eppendorf vial.

Next, 13 μL of each compound (**DFO**, **12a**, **12b**, **12c** [4 mg/mL in DMSO] and C2HOPO [**13d**]) was added to 300 μL of 1% BSA in PBS in each of five Eppendorf vials. The vials were incubated at 37 °C for 1 h. After 1 h, the contents of each vial were transferred to five different cassettes and rotated in 350 mL of 0.1 M NH_4OAc. The buffer was changed every 3 h twice. After three buffer washes, the cassettes were taken out, transferred into an Eppendorf vial, and stored at 4 °C for labeling experiments.

Conjugation of Chelators to Anti-PD-L1 Antibodies. The anti-PD-L1 antibodies STM004 and STM108 (STCube Pharmaceuticals, Gaithersburg, MD) were conjugated with DFO and HOPO in 0.1 M $NaHCO_3$ solution (pH 8.4). Two cassettes were soaked in 0.1 M $NaHCO_3$ (350 mL) for 10 min, then 300 μL each of STM004 (3.52 mg/mL) or STM108 (3.01 mg/mL) was injected into two cassettes, which were placed in two separate beakers, each containing 350 mL of 0.1 M $NaHCO_3$. The cassettes were rotated for 3 h at 4 °C. After 3 h, 0.1 M $NaHCO_3$ buffer was replaced twice at an interval of 3 h. The cassettes were taken out, and STM004 and STM108 were

https://doi.org/10.1021/acsomega.3c01547
ACS Omega 2023, 8, 17181−17194

recovered into two separate Eppendorf vials. Similar procedures were used for all HOPO derivative conjugations.

Next, 13 μL of DFO (3 mg/mL in DMSO) was added to 300 μL of STM004 or STM108 (buffer-exchanged vial) into each of the two Eppendorf vials. The vials were incubated at 37 °C for 1 h. After 1 h, the contents of each vial were transferred to two different cassettes, which were rotated in 350 mL of 0.1 M NH_4OAc at 4 °C. The buffer was changed every 3 h thrice. After three buffer washes, the cassettes were taken out, transferred into two Eppendorf vials, and stored at 4 °C for labeling experiments.

Then, 29 μL each of compounds **12a**, **12b**, and **12c** (3 mg/mL in DMSO, pH adjusted to 7.0) was added to 300 μL of STM004 or STM108 (buffer-exchanged vial) into each of six Eppendorf vials. All six vials were incubated at 37 °C for 1 h. After 1 h, the contents of each vial were transferred to six different cassettes and rotated in 350 mL of 0.1 M NH_4OAc at 4 °C. The buffer was changed every 3 h thrice. After three buffer washes, the cassettes were taken out, transferred into six Eppendorf vials, and stored at 4 °C for labeling experiments.

Radiolabeling. ^{89}Zr was received as ^{89}Zr oxalate in 1.0 M oxalic acid from the MD Anderson Cyclotron Facility. This solution was neutralized with 1 M sodium carbonate to pH 7.0. Stock solutions of both HOPO (0.25 M) and DFO ligands (0.33 M) were prepared. Dilutions were made using 50 μL of each ligand and 950 μL of 0.1 M ammonium acetate at pH 7.0 (0.172 μM). HOPO and DFO ligands were labeled by mixing 100 μL of dilute solutions of each ligand with the neutralized ^{89}Zr solution at room temperature for 1 to 3 h. Samples were labeled with 600 to 800 μCi of activity. Reactions were monitored using radio-TLC with ITLC-SA strips (Agilent Technologies) and 50 mM EDTA at pH 7.0 as the mobile phase. ^{89}Zr-ligand complexes remained at the origin, while free ^{89}Zr was scavenged with EDTA in the mobile phase.

Stability Studies. All of the ^{89}Zr-DFO-BSA and ^{89}Zr-HOPO-BSA complexes were tested for their thermal stability at different temperatures (4 °C, room temperature, and 37 °C). For each ^{89}Zr complex, three sets of samples were made, consisting of 225 μL of PBS (pH 7.4) and 25 μL (10 μCi) of the ^{89}Zr-ligand-BSA complexes. The sample sets were kept at different temperatures in triplicate for each temperature. The thermal stability of the samples was monitored using radio-TLC before being added to the PBS and every 24 h for up to 48 h of incubation. The stability of the complexes was based on the percentage of ^{89}Zr that was retained at the origin of TLC. For the EDTA challenge test of ^{89}Zr-ligand complexes, complexes were incubated with a 10-fold excess of ethylenediamine tetraacetic acid (EDTA) at pH 5, 6, 7, and 8, at 37 °C for 7 days. Subsequently, the stability of the complexes was monitored by radio-TLC every 24 hours for 7 days post initial incubation. Similarly, the pH stability of ^{89}Zr-DFO-STM004, ^{89}Zr-DFO-STM108, ^{89}Zr-C5HOPO-STM004, and ^{89}Zr-C5HOPO-STM108 was evaluated at 37 °C in PBS at pH 5, 6, 7 and 8 over 7 days by radio-TLC.

Serum Stability Studies. ^{89}Zr-ligand-BSA complexes were prepared according to a previously published radiolabeling procedure.[35] For each ^{89}Zr complex, sample sets were made consisting of 450 μL of 100% human serum and 50 μL of the ^{89}Zr-DFO-BSA complexes as one set and 450 μL of 100% mouse serum and 50 μL of ^{89}Zr-HOPO-BSA complexes as the other set. The samples were placed in a heat block at 37 °C with occasional shaking. The stability of the samples was monitored using radio-TLC before they were added to the serum and then every 24 h for up to 72 h of incubation. The stability of the complexes was measured based on the percentage of ^{89}Zr that was retained at the origin of TLC. Three samples were prepared for each complex to obtain triplicate data.

Live Cell Binding Assay of ^{89}Zr-Labeled Antibodies. Live cell binding assays were performed according to a previously reported procedure with modifications.[57−59] 24 hours before the planned binding assay, BT549 cells were plated directly into six-well clear-bottom plastic plates at a density of 10^6 cells per well in DMEM (2 mL) supplemented with F12 (total of 9 plates for each labeled antibody experiment: 3 for BT549 knockout, 3 for BT549 WT for blocking, and 3 for BT549 WT with cells attached, not a suspension). The cells were about 80−90% confluence after 24 h. At 1 h prior to the binding experiment, the culture medium was changed to 2 mL of pre-warmed (37 °C with CO_2) DMEM (pH 7.4 at 37 °C) per well and the plates were incubated for 1 h to allow the cells to equilibrate in the new medium. For the blocking experiment, unlabeled (cold) monoclonal antibody (STM004 or STM108, 3.52 or 3.54 mg/mL, respectively) was added to three wells as 9 μL (50X excess). After 20 min, ^{89}Zr-labeled antibody in DMEM buffer (1 μCi in 30 μL DMEM) was added to each well plate containing 2 mL of MEBSS. Plates were gently agitated on a flat surface in forward-backward, left-right, and diagonal directions several times before placing plates back in the incubator at 37 °C with CO_2 for 1 h. After 1 h, the plates were placed on ice. 1 mL of supernatant was removed, and activity was measured on a γ counter. These values were recorded as extracellular space counts. The remaining supernatants were then aspirated, and the wells were washed with 1 mL of ice-cold DMEM buffer (pH 7.4 at 4 °C) and aspirated with DMEM three times. For extraction of protein from lysates, lysis buffer solution (2.5 mL of 1% SDS and 10 mM sodium borate) was added to each well and pipetted up and down several times. Proteins were extracted for 30 min at room temperature, and 100 μL of lysate was collected from each well. Tracer activity was counted on a γ counter. The remaining lysates were stored at −80 °C for protein assays. Protein concentration was measured after complete decay of activity using a BCA assay.

Immunofluorescence Assay of STM004 and STM108 Cellular Binding. Ten thousand cells were plated in 300 μL of complete media on eight-well chamber slides. 24 h later, 10 μg/mL of the relevant antibody (STM004 or STM108 alone, or antibodies conjugated to DFO or HOPO) were added to the cells and incubated for 24 h in a 37 °C incubator with 5% CO_2. The cells were fixed with 4% paraformaldehyde for 20 min, then permeabilized with 0.1% Triton X-100 for 5 min at room temperature, and blocked with 3% BSA for 30 min at room temperature. The cells were then incubated for 1 h at room temperature with a 1:50 dilution of RPE-labeled secondary antibody and a 1:100 dilution of Alexa Fluor 488-Phalloidin in a 1.5% BSA solution. The cells were then incubated for 15 min with a 1:10000 dilution of DAPI in PBS at room temperature. Slides were mounted with prolonged diamond antifade mount overnight at 4 °C. The cells were imaged with a Nikon Eclipse Ti microscope using a Hamamatsu camera and the 40x objective. Exposure windows and times were as follows: GFP 500 ms, TRITC 500 ms, and DAPI 1 s. Image quantification was conducted using an in-house script implemented in Matlab R2019b. Nikon nd2 images were read using Bio-format. The average intensity of at least five fields per condition was calculated by dividing the mean intensity of the TRITC image

https://doi.org/10.1021/acsomega.3c01547
ACS Omega 2023, 8, 17181−17194

by the number of nuclei in the field. Nuclei were counted using an implementation of the watershed transformation.

Biodistribution Studies. *In vivo* biodistribution studies of ^{89}Zr-labeled DFO-BSA, ^{89}Zr-labeled C2HOPO-BSA, and C3-C5HOPO-BSA complexes were performed in healthy athymic nude mice. The mice (n = 4 for each protein) were injected with ^{89}Zr-DFO-BSA (25−35 μCi), ^{89}Zr-C2HOPO-BSA or C3-C5HOPO-BSA complexes (25−30 μCi) in PBS *via* the tail vein. After injection, the mice underwent PET imaging every 24 h for up to 48 h. After 48 h, the mice were euthanized by CO_2 (g) asphyxiation. The blood, muscle, bone, heart, lung, liver, spleen, pancreas, intestine, stomach, and kidney were removed, weighed, and assayed for radioactivity on a γ counter calibrated for ^{89}Zr. Similarly, all of the ^{89}Zr-labeled DFO-STM004, DFO-STM108 (25−30 μCi), or ^{89}Zr-labeled C5HOPO-STM004 or C5HOPO-STM108 (12−14 μCi) radioimmuno conjugates were injected into mice bearing BT-549 TNBC xenograft tumors (n = 4 for each antibody). The mice underwent PET imaging at 24 h, either 48 or 72, and 144 h. After 144 h, all of the mice were euthanized by CO_2 (g) asphyxiation. The blood, muscle, bone, heart, lung, liver, spleen, pancreas, intestine, stomach, kidney, and tumor were removed, weighed, and assayed for radioactivity using a γ counter calibrated for ^{89}Zr. For all radio-conjugates, γ counts were converted into activity using a calibration curve generated from an ^{89}Zr standard. Count data were corrected for background and decay at the time of injection, and the percent injected dose per gram (%ID/g) for each tissue sample was calculated relative to the total activity injected.

Bone Marrow Isolation. To quantify bone uptake of ^{89}Zr tracer after biodistribution, bones from all of the experimental animals were soaked in 2 mL of SDS solution (20% w/v) for 30 min in individual tissue culture dishes (40 mm × 110 mm). SDS was blotted off, and the bone marrow was extracted using a 25-gauge ×1 needle into a γ-counting tube. A γ counter was used to quantify ^{89}Zr activity in bone and bone marrow (n = 4 for each radio-conjugate).

Statistical Analysis. All data are presented as mean ± standard deviation. Statistical analysis was performed using GraphPad Prism version 7.03 for Windows. Differences in ^{89}Zr activity in live cell binding assays were tested for significance using unpaired Student's t-tests and ordinary one-way ANOVA. P values <0.05 were considered significant.

■ ASSOCIATED CONTENT

Supporting Information

The Supporting Information is available free of charge at https://pubs.acs.org/doi/10.1021/acsomega.3c01547.

Synthetic schemes and detailed experimental procedures, HPLC chromatograms, ^{1}H NMR, ^{13}C NMR, electrospray ionization (ESI), and HRMS data (PDF)

■ AUTHOR INFORMATION

Corresponding Author

David Piwnica-Worms − *Department of Cancer Systems Imaging, The University of Texas MD Anderson Cancer Center, Houston, Texas 77030, United States;* orcid.org/0000-0002-2120-7217; Phone: 713-745-8521; Email: dpiwnica-worms@mdanderson.org; Fax: 713-794-5456

Authors

Bhasker Radaram − *Department of Cancer Systems Imaging, The University of Texas MD Anderson Cancer Center, Houston, Texas 77030, United States;* Present Address: Bioimaging, GlaxoSmithKline, Collegeville, Pennsylvania 19426, United States

Sarah E. Glazer − *Department of Cancer Systems Imaging, The University of Texas MD Anderson Cancer Center, Houston, Texas 77030, United States;* Present Address: Department of Medicine, School of Medicine, Oregan Health Sciences University, Portland, Oregon 97239, United States

Ping Yang − *Department of Cancer Systems Imaging, The University of Texas MD Anderson Cancer Center, Houston, Texas 77030, United States*

Chia-Wei Li − *Department of Molecular & Cellular Oncology, The University of Texas MD Anderson Cancer Center, Houston, Texas 77030, United States;* Present Address: Institute of Biomedical Sciences, Academia Sinica, Taipei 115, Taiwan; orcid.org/0000-0002-2531-2866

Mien-Chie Hung − *Department of Molecular & Cellular Oncology, The University of Texas MD Anderson Cancer Center, Houston, Texas 77030, United States;* Present Address: Graduate Institute of Biomedical Sciences, China Medical University, Taichung 406, Taiwan

Seth T. Gammon − *Department of Cancer Systems Imaging, The University of Texas MD Anderson Cancer Center, Houston, Texas 77030, United States;* orcid.org/0000-0001-8647-0975

Mian Alauddin − *Department of Cancer Systems Imaging, The University of Texas MD Anderson Cancer Center, Houston, Texas 77030, United States;* Present Address: Department of Pathology, Keck School of Medicine, University of Southern California, Los Angeles, California 90033, United States

Complete contact information is available at: https://pubs.acs.org/10.1021/acsomega.3c01547

Author Contributions

○B.R. and S.E.G. contributed equally to this work. B.R. executed chemical synthesis, chelate conjugation and radiolabeling, and *in vitro* tracer assays; contributed to animal studies and *ex vivo* biodistribution; quantified and analyzed data; and provided a first draft of the manuscript. S.E.G. executed fluorescence labeling and cellular bioassays, quantified and analyzed data, and co-wrote the manuscript. P.Y. executed and assisted with cellular and *in vivo* experiments. C.-W.L. and M.-C.H. provided reagents and edited the manuscript. S.T.G. assisted with imaging analysis and statistical analysis and edited the manuscript. M.A. supervised chemical studies and edited the manuscript. D.P.-W. supervised the study, analyzed data, provided resources, and edited the manuscript.

Notes

The authors declare the following competing financial interest(s): C.-W.L and M.-C.H. are listed inventors on patent applications for the antibodies contained herein. The remaining authors declare no conflicts of interest.

■ ACKNOWLEDGMENTS

The authors thank Federica Pisaneschi for helpful discussions and review of the manuscript, Vien Long and Laura Bover from the Antibody Core Facility at the University of Texas MD Anderson Cancer Center for maintaining stocks of STM004 and

STM108 antibodies, and the Scientific Publication Services in the Research Medical Library at MD Anderson for editing the manuscript. This work was supported by the U.S. National Institutes of Health MD Anderson Cancer Center-Washington University Inter-Institutional Molecular Imaging Center Grant (P50 CA94056; D.P-W), the MD Anderson Cancer Center Support Grant (P30 CA016672), which supports the NMR Facility and Small Animal Imaging Facility, and by a U.S. National Institutes of Health Fellowship Grant (NCI F30 CA239332, S.E.G.). This work was funded in part by the Ministry of Science and Technology (MOST 109-2314-B-001-002; C.-W.L).

■ ABBREVIATIONS

PD-L1, programmed death ligand 1; PD-1, programmed death-1; PET, positron emission tomography; DFO, desferrioxamine B; HOPO, hydroxypyridinone; BSA, bovine serum albumin; DCM, dichloromethane; NMR, nuclear magnetic resonance; HRMS, high-resolution mass spectrometry; HPLC, high-performance liquid chromatography; TLC, thin-layer chromatography; PBS, phosphate-buffered saline; DMEM, Dulbecco's modified Eagle's medium; SDS, sodium dodecyl sulfate; BCA, bicinchoninic acid; MEBSS, modified Earle's balanced salt solution; WT, wild type; cpm, counts per minute; CT, computed tomography; %ID/g, percent injected dose per gram; DMSO, dimethyl sulfoxide; ITLC, instant thin-layer chromatography; DMF, dimethylformamide; TFA, trifluoroacetic acid

■ REFERENCES

(1) Curiel, T. J.; Wei, S.; Dong, H.; Alvarez, X.; Cheng, P.; Mottram, P.; Krzysiek, R.; Knutson, K. L.; Daniel, B.; Zimmermann, M. C.; et al. Blockade of B7-H1 improves myeloid dendritic cell−mediated antitumor immunity. *Nat. Med.* **2003**, *9*, 562−567.

(2) Freeman, G. J.; Long, A. J.; Iwai, Y.; Bourque, K.; Chernova, T.; Nishimura, H.; Fitz, L. J.; Malenkovich, N.; Okazaki, T.; Byrne, M. C.; et al. Engagement of the Pd-1 Immunoinhibitory Receptor by a Novel B7 Family Member Leads to Negative Regulation of Lymphocyte Activation. *J. Exp. Med.* **2000**, *192*, 1027−1034.

(3) Li, C.-W.; Lim, S.-O.; Xia, W.; Lee, H.-H.; Chan, L.-C.; Kuo, C.-W.; Khoo, K.-H.; Chang, S.-S.; Cha, J.-H.; Kim, T.; et al. Glycosylation and stabilization of programmed death ligand-1 suppresses T-cell activity. *Nat. Commun.* **2016**, *7*, No. 12632.

(4) Brahmer, J. R.; Drake, C. G.; Wollner, I.; Powderly, J. D.; Picus, J.; Sharfman, W. H.; Stankevich, E.; Pons, A.; Salay, T. M.; McMiller, T. L.; et al. Phase I Study of Single-Agent Anti−Programmed Death-1 (MDX-1106) in Refractory Solid Tumors: Safety, Clinical Activity, Pharmacodynamics, and Immunologic Correlates. *J. Clin. Oncol.* **2010**, *28*, 3167−3175.

(5) Sznol, M.; Chen, L. Antagonist Antibodies to PD-1 and B7-H1 (PD-L1) in the Treatment of Advanced Human Cancer. *Clin. Cancer Res.* **2013**, *19*, 1021−1034.

(6) Akinleye, A.; Rasool, Z. Immune checkpoint inhibitors of PD-L1 as cancer therapeutics. *J. Hematol. Oncol.* **2019**, *12*, No. 92.

(7) Acurcio, R. C.; Pozzi, S.; Carreira, B.; Pojo, M.; Gomez-Cebrian, N.; Casimiro, S.; Fernandes, A.; Barateiro, A.; Farricha, V.; Brito, J.; et al. Therapeutic targeting of PD-1/PD-L1 blockade by novel small-molecule inhibitors recruits cytotoxic T cells into solid tumor microenvironment. *J. ImmunoTher. Cancer* **2022**, *10*, No. e004695.

(8) Pardoll, D. M. The blockade of immune checkpoints in cancer immunotherapy. *Nat. Rev. Cancer* **2012**, *12*, 252−264.

(9) Wei, S. C.; Duffy, C. R.; Allison, J. P. Fundamental Mechanisms of Immune Checkpoint Blockade Therapy. *Cancer Discovery* **2018**, *8*, 1069−1086.

(10) Postow, M. A.; Callahan, M. K.; Wolchok, J. D. Immune Checkpoint Blockade in Cancer Therapy. *J. Clin. Oncol.* **2015**, *33*, 1974−1982.

(11) Zanello, A.; Bortolotti, M.; Maiello, S.; Bolognesi, A.; Polito, L. Anti-PD-L1 immunoconjugates for cancer therapy: Are available antibodies good carriers for toxic payload delivering? *Front. Pharmacol.* **2022**, *13*, No. 3142.

(12) Malmberg, R.; Zietse, M.; Dumoulin, D. W.; Hendrikx, J.; Aerts, J.; van der Veldt, A. A. M.; Koch, B. C. P.; Sleijfer, S.; van Leeuwen, R. W. F. Alternative dosing strategies for immune checkpoint inhibitors to improve cost-effectiveness: a special focus on nivolumab and pembrolizumab. *Lancet Oncol.* **2022**, *23*, e552−e561.

(13) Kovács, S. A.; Gyorffy, B. Transcriptomic datasets of cancer patients treated with immune-checkpoint inhibitors: a systematic review. *J. Transl. Med.* **2022**, *20*, No. 249.

(14) Schmid, P.; Rugo, H. S.; Adams, S.; Schneeweiss, A.; Barrios, C. H.; Iwata, H.; Diéras, V.; Henschel, V.; Molinero, L.; Chui, S. Y.; et al. Atezolizumab plus nab-paclitaxel as first-line treatment for unresectable, locally advanced or metastatic triple-negative breast cancer (IMpassion130): updated efficacy results from a randomised, double-blind, placebo-controlled, phase 3 trial. *Lancet Oncol.* **2020**, *21*, 44−59.

(15) Varma, R.; Wright, M.; Abraham, J.; Kruse, M. Immune checkpoint inhibition in early-stage triple-negative breast cancer. *Expert Rev. Anticancer Ther.* **2022**, *22*, 1225−1238.

(16) Mortezaee, K.; Majidpoor, J. Transforming growth factor-beta signalling in tumour resistance to the anti-PD-(L)1 therapy: Updated. *J. Cell. Mol. Med.* **2023**, *27*, 311−321.

(17) Li, L.; Zhang, F.; Liu, Z.; Fan, Z. Immunotherapy for Triple-Negative Breast Cancer: Combination Strategies to Improve Outcome. *Cancers* **2023**, *15*, No. 321.

(18) Patel, K. K.; Hassan, D.; Nair, S.; Tejovath, S.; Kahlon, S. S.; Peddemul, A.; Sikandar, R.; Mostafa, J. A. Role of Immunotherapy in the Treatment of Triple-Negative Breast Cancer: A Literature Review. *Cureus* **2022**, *14*, No. e31729.

(19) Topalian, S. L.; Taube, J. M.; Anders, R. A.; Pardoll, D. M. Mechanism-driven biomarkers to guide immune checkpoint blockade in cancer therapy. *Nat. Rev. Cancer* **2016**, *16*, 275−287.

(20) Marciscano, A. E.; Thorek, D. L. J. Role of noninvasive molecular imaging in determining response. *Adv. Radiat. Oncol.* **2018**, *3*, 534−547.

(21) Christensen, C.; Kristensen, L. K.; Alfsen, M. Z.; Nielsen, C. H.; Kjaer, A. Quantitative PET imaging of PD-L1 expression in xenograft and syngeneic tumour models using a site-specifically labelled PD-L1 antibody. *Eur. J. Nucl. Med. Mol. Imaging* **2020**, *47*, 1302−1313.

(22) Donnelly, D. J.; Smith, R. A.; Morin, P.; Lipovšek, D.; Gokemeijer, J.; Cohen, D.; Lafont, V.; Tran, T.; Cole, E. L.; Wright, M.; et al. Synthesis and Biologic Evaluation of a Novel 18F-Labeled Adnectin as a PET Radioligand for Imaging PD-L1 Expression. *J. Nucl. Med.* **2018**, *59*, 529−535.

(23) Truillet, C.; Oh, H. L. J.; Yeo, S. P.; Lee, C.-Y.; Huynh, L. T.; Wei, J.; Parker, M. F. L.; Blakely, C.; Sevillano, N.; Wang, Y.-H.; et al. Imaging PD-L1 Expression with ImmunoPET. *Bioconjugate Chem.* **2018**, *29*, 96−103.

(24) Lesniak, W. G.; Chatterjee, S.; Gabrielson, M.; Lisok, A.; Wharram, B.; Pomper, M. G.; Nimmagadda, S. PD-L1 Detection in Tumors Using [64Cu]Atezolizumab with PET. *Bioconjugate Chem.* **2016**, *27*, 2103−2110.

(25) Li, D.; Cheng, S.; Zou, S.; Zhu, D.; Zhu, T.; Wang, P.; Zhu, X. Immuno-PET Imaging of 89Zr Labeled Anti-PD-L1 Domain Antibody. *Mol. Pharm.* **2018**, *15*, 1674−1681.

(26) Yoon, J. K.; Park, B. N.; Ryu, E. K.; An, Y. S.; Lee, S. J. Current Perspectives on (89)Zr-PET Imaging. *Int. J. Mol. Sci.* **2020**, *21*, No. 4309.

(27) Verhoeff, S. R.; van den Heuvel, M. M.; van Herpen, C.M.L.; Piet, B.; Aarntzen, E.; Heskamp, S. Programmed Cell Death-1/Ligand-1 PET Imaging: A Novel Tool to Optimize Immunotherapy? *PET Clin.* **2020**, *15*, 35−43.

(28) van der Veen, E. L.; Giesen, D.; Jong, L. P.-d.; Jorritsma-Smit, A.; De Vries, E.G.E.; Lub-de Hooge, M. N. (89)Zr-pembrolizumab biodistribution is influenced by PD-1-mediated uptake in lymphoid organs. *J. ImmunoTher. Cancer* **2020**, *8*, No. e000938.

(29) Rubins, D. J.; Meng, X.; McQuade, P.; Klimas, M.; Getty, K.; Lin, S. A.; Connolly, B. M.; O'Malley, S. S.; Haley, H.; Purcell, M.; et al. In

https://doi.org/10.1021/acsomega.3c01547
ACS Omega 2023, 8, 17181−17194

Vivo Evaluation and Dosimetry Estimate for a High Affinity Affibody PET Tracer Targeting PD-L1. *Mol. Imaging Biol* **2021**, *23*, 241−249.
(30) Nienhuis, P. H.; Antunes, I. F.; Glaudemans, A.; Jalving, M.; Leung, D.; Noordzij, W.; Slart, R.; de Vries, E.F.J.; Hospers, G.A.P. (18)F-BMS986192 PET Imaging of PD-L1 in Metastatic Melanoma Patients with Brain Metastases Treated with Immune Checkpoint Inhibitors: A Pilot Study. *J. Nucl. Med.* **2022**, *63*, 899−905.
(31) Boers, J.; de Vries, E. F. J.; Glaudemans, A.; Hospers, G. A. P.; Schroder, C. P. Application of PET Tracers in Molecular Imaging for Breast Cancer. *Curr. Oncol. Rep.* **2020**, *22*, No. 85.
(32) Wei, W.; Rosenkrans, Z. T.; Liu, J.; Huang, G.; Luo, Q.-Y.; Cai, W. ImmunoPET: Concept, Design, and Applications. *Chem. Rev.* **2020**, *120*, 3787−3851.
(33) Deri, M. A.; Zeglis, B. M.; Francesconi, L. C.; Lewis, J. S. PET imaging with 89Zr: From radiochemistry to the clinic. *Nucl. Med. Biol.* **2013**, *40*, 3−14.
(34) Vugts, D. J.; van Dongen, G. A. M. S. 89Zr-labeled compounds for PET imaging guided personalized therapy. *Drug Discovery Today: Technol.* **2011**, *8*, e53−e61.
(35) Deri, M. A.; Ponnala, S.; Zeglis, B. M.; Pohl, G.; Dannenberg, J. J.; Lewis, J. S.; Francesconi, L. C. Alternative Chelator for 89Zr Radiopharmaceuticals: Radiolabeling and Evaluation of 3,4,3-(LI-1,2-HOPO). *J. Med. Chem.* **2014**, *57*, 4849−4860.
(36) Verhoeff, S. R.; van Es, S. C.; Boon, E.; van Helden, E.; Angus, L.; Elias, S. G.; Oosting, S. F.; Aarntzen, E. H.; Brouwers, A. H.; Kwee, T. C.; et al. Lesion detection by [(89)Zr]Zr-DFO-girentuximab and [(18)F]FDG-PET/CT in patients with newly diagnosed metastatic renal cell carcinoma. *Eur. J. Nucl. Med. Mol. Imaging* **2019**, *46*, 1931−1939.
(37) Qiu, K.; Zhao, Q.; Wang, J.; Qi, G. H.; Wu, S. G.; Zhang, H. J. Effects of Pyrroloquinoline Quinone on Lipid Metabolism and Anti-Oxidative Capacity in a High-Fat-Diet Metabolic Dysfunction-Associated Fatty Liver Disease Chick Model. *Int. J. Mol. Sci.* **2021**, *22*, No. 1458.
(38) Lee, Y. J.; van den Berg, N. S.; Duan, H.; Azevedo, E. C.; Ferri, V.; Hom, M.; Raymundo, R. C.; Valencia, A.; Castillo, J.; Shen, B.; et al. 89Zr-panitumumab Combined With 18F-FDG PET Improves Detection and Staging of Head and Neck Squamous Cell Carcinoma. *Clin. Cancer Res.* **2022**, *28*, 4425−4434.
(39) de Ruijter, L. K.; van de Donk, P. P.; Hooiveld-Noeken, J. S.; Giesen, D.; Elias, S. G.; Hooge, M. N. L.-d.; Oosting, S. F.; Jalving, M.; Timens, W.; Brouwers, A. H.; et al. Whole-body CD8(+) T cell visualization before and during cancer immunotherapy: a phase 1/2 trial. *Nat. Med.* **2022**, *28*, 2601−2610.
(40) Carrasquillo, J. A.; Fine, B. M.; Pandit-Taskar, N.; Larson, S. M.; Fleming, S. E.; Fox, J. J.; Cheal, S. M.; O'Donoghue, J. A.; Ruan, S.; Ragupathi, G.; et al. Imaging Patients with Metastatic Castration-Resistant Prostate Cancer Using (89)Zr-DFO-MSTP2109A Anti-STEAP1 Antibody. *J. Nucl. Med.* **2019**, *60*, 1517−1523.
(41) Price, E. W.; Orvig, C. Matching chelators to radiometals for radiopharmaceuticals. *Chem. Soc. Rev.* **2014**, *43*, 260−290.
(42) Lewis, J. S.; Windhorst, A. D.; Zeglis, B. M. *Radiopharmaceutical Chemistry*; Springer International Publishing Imprint: Switzerland, 2019; Vol. *1*, pp 1−651.
(43) Verel, I.; Visser, G. W. M.; Boellaard, R.; Stigter-van Walsum, M.; Snow, G. B.; van Dongen, G. A. M. S. 89Zr Immuno-PET: Comprehensive Procedures for the Production of 89Zr-Labeled Monoclonal Antibodies. *J. Nucl. Med.* **2003**, *44*, 1271−1281.
(44) Perk, L. R.; Vosjan, M. J. W. D.; Visser, G. W. M.; Budde, M.; Jurek, P.; Kiefer, G. E.; van Dongen, G. A. M. S. p-Isothiocyanatobenzyl-desferrioxamine: a new bifunctional chelate for facile radiolabeling of monoclonal antibodies with zirconium-89 for immuno-PET imaging. *Eur. J. Nucl. Med. Mol. Imaging* **2010**, *37*, 250−259.
(45) Raavé, R.; Sandker, G.; Adumeau, P.; Jacobsen, C. B.; Mangin, F.; Meyer, M.; Moreau, M.; Bernhard, C.; Da Costa, L.; Dubois, A.; et al. Direct comparison of the in vitro and in vivo stability of DFO, DFO* and DFOcyclo* for 89Zr-immunoPET. *Eur. J. Nucl. Med. Mol. Imaging* **2019**, *46*, 1966−1977.
(46) Deri, M. A.; Ponnala, S.; Kozlowski, P.; Burton-Pye, B. P.; Cicek, H. T.; Hu, C.; Lewis, J. S.; Francesconi, L. C. p-SCN-Bn-HOPO: A Superior Bifunctional Chelator for 89Zr ImmunoPET. *Bioconjugate Chem.* **2015**, *26*, 2579−2591.
(47) Hudis, C. A. Trastuzumab — Mechanism of Action and Use in Clinical Practice. *N. Engl. J. Med.* **2007**, *357*, 39−51.
(48) de Goeij, B. E. C. G.; Peipp, M.; de Haij, S.; van den Brink, E. N.; Kellner, C.; Riedl, T.; de Jong, R.; Vink, T.; Strumane, K.; Bleeker, W. K.; Parren, P. W. HER2 monoclonal antibodies that do not interfere with receptor heterodimerization-mediated signaling induce effective internalization and represent valuable components for rational antibody-drug conjugate design. *mAbs* **2014**, *6*, 392−402.
(49) Tinianow, J. N.; Pandya, D. N.; Pailloux, S. L.; Ogasawara, A.; Vanderbilt, A. N.; Gill, H. S.; Williams, S. P.; Wadas, T. J.; Magda, D.; Marik, J. Evaluation of a 3-hydroxypyridin-2-one (2,3-HOPO) Based Macrocyclic Chelator for (89)Zr(4+) and Its Use for ImmunoPET Imaging of HER2 Positive Model of Ovarian Carcinoma in Mice. *Theranostics* **2016**, *6*, 511−521.
(50) Li, C.-W.; Lim, S.-O.; Chung, E. M.; Kim, Y.-S.; Park, A. H.; Yao, J.; Cha, J.-H.; Xia, W.; Chan, L.-C.; Kim, T.; et al. Eradication of Triple-Negative Breast Cancer Cells by Targeting Glycosylated PD-L1. *Cancer Cell* **2018**, *33*, 187−201.e10.
(51) Bhupathiraju, N. V. S. D. K.; Younes, A.; Cao, M.; Ali, J.; Cicek, H. T.; Tully, K. M.; Ponnala, S.; Babich, J. W.; Deri, M. A.; Lewis, J. S.; et al. Improved synthesis of the bifunctional chelator p-SCN-Bn-HOPO. *Org. Biomol. Chem.* **2019**, *17*, 6866−6871.
(52) Perera, S.; Radaram, B. Piwnica-Worms. D.; Alauddin, M. M. Poster Presentations. *J. Labelled Compd. Radiopharm.* **2017**, *60*, 111−640.
(53) Vosjan, M. J. W. D.; Perk, L. R.; Visser, G. W. M.; Budde, M.; Jurek, P.; Kiefer, G. E.; van Dongen, G. A. M. S. Conjugation and radiolabeling of monoclonal antibodies with zirconium-89 for PET imaging using the bifunctional chelate p-isothiocyanatobenzyl-desferrioxamine. *Nat. Protoc.* **2010**, *5*, 739−743.
(54) Sharma, S. K.; Chow, A.; Monette, S.; Vivier, D.; Pourat, J.; Edwards, K. J.; Dilling, T. R.; Abdel-Atti, D.; Zeglis, B. M.; Poirier, J. T.; Lewis, J. S. Fc-Mediated Anomalous Biodistribution of Therapeutic Antibodies in Immunodeficient Mouse Models. *Cancer Res.* **2018**, *78*, 1820−1832.
(55) Bruhns, P.; Jönsson, F. Mouse and human FcR effector functions. *Immunol. Rev.* **2015**, *268*, 25−51.
(56) Nimmerjahn, F.; Ravetch, J. V. Fcgamma receptors: old friends and new family members. *Immunity* **2006**, *24*, 19−28.
(57) Sharma, V.; Sivapackiam, J.; Harpstrite, S. E.; Prior, J. L.; Gu, H.; Rath, N. P.; Piwnica-Worms, D. A Generator-Produced Gallium-68 Radiopharmaceutical for PET Imaging of Myocardial Perfusion. *PLoS One* **2014**, *9*, No. e109361.
(58) Sharma, V.; Beatty, A.; Wey, S. P.; Dahlheimer, J.; Pica, C. M.; Crankshaw, C. L.; Bass, L.; Green, M. A.; Welch, M. J.; Piwnica-Worms, D. Novel gallium(III) complexes transported by MDR1 P-glycoprotein: potential PET imaging agents for probing P-glycoprotein-mediated transport activity in vivo. *Chem. Biol.* **2000**, *7*, 335−343.
(59) Radaram, B.; Pisaneschi, F.; Rao, Y.; Yang, P.; Piwnica-Worms, D.; Alauddin, M. M. Novel derivatives of anaplastic lymphoma kinase inhibitors: Synthesis, radiolabeling, and preliminary biological studies of fluoroethyl analogues of crizotinib, alectinib, and ceritinib. *Eur. J. Med. Chem.* **2019**, *182*, No. 111571.

https://doi.org/10.1021/acsomega.3c01547
ACS Omega 2023, 8, 17181−17194